Appl Phys B (2009) 96: 161–173
DOI 10.1007/s00340-009-3446-7

Applied Physics B
Lasers and Optics

Sensitive detection of temperature behind reflected shock waves using wavelength modulation spectroscopy of CO_2 near 2.7 μm

A. Farooq · J.B. Jeffries · R.K. Hanson

Received: 26 November 2008 / Published online: 5 March 2009

Abstract Tunable diode-laser absorption of CO_2 near 2.7 μm incorporating wavelength modulation spectroscopy with second-harmonic detection (WMS-2f) is used to provide a new sensor for sensitive and accurate measurement of the temperature behind reflected shock waves in a shock-tube. The temperature is inferred from the ratio of 2f signals for two selected absorption transitions, at 3633.08 and 3645.56 cm^{-1}, belonging to the $\nu_1 + \nu_3$ combination vibrational band of CO_2 near 2.7 μm. The modulation depths of 0.078 and 0.063 cm^{-1} are optimized for the target conditions of the shock-heated gases ($P \sim 1$–2 atm, $T \sim 800$–1600 K). The sensor is designed to achieve a high sensitivity to the temperature and a low sensitivity to cold boundary-layer effects and any changes in gas pressure or composition. The fixed-wavelength WMS-2f sensor is tested for temperature and CO_2 concentration measurements in a heated static cell (600–1200 K) and in non-reactive shock-tube experiments (900–1700 K) using CO_2–Ar mixtures. The relatively large CO_2 absorption strength near 2.7 μm and the use of a WMS-2f strategy minimizes noise and enables measurements with lower concentration, higher accuracy, better sensitivity and improved signal-to-noise ratio (SNR) relative to earlier work, using transitions in the 1.5 and 2.0 μm CO_2 combination bands. The standard deviation of the measured temperature histories behind reflected shock waves is less than 0.5%. The temperature sensor is also demonstrated in reactive shock-tube experiments of n-heptane oxidation. Seeding of relatively inert CO_2 in the initial fuel-oxidizer mixture is utilized to enable measurements of the pre-ignition temperature profiles. To our knowledge, this work represents the first application of wavelength modulation spectroscopy to this new class of diode lasers near 2.7 μm.

PACS 42.62.Fi · 42.55.Px · 07.07.Df

1 Introduction

The design and optimization of combustion systems relies heavily on accurate predictive modeling. These combustion models provide information regarding performance such as efficiency and pollutant emissions [1]. An important component of any combustion model is the reaction mechanism that describes the chemistry of the combustion event. The constitution of a reaction mechanism requires a database of accurate chemical reaction rate constants for the temperature range of interest. The test of the performance of such a mechanism requires careful experiments to determine ignition times and species concentration time histories in reacting or combusting flow with well-controlled temperature, pressure, and reaction time. Shock-tubes can provide well-defined initial temperatures and pressures for such kinetic investigations [2]. While ignition delay times provide an overall measure of the performance of kinetic mechanisms, refinement and validation of the detailed chemistry of the system requires a time-dependent picture of temperature and the species concentrations [2]. Laser absorption diagnostics can provide these data for shock-tube experiments. Here, we report an improved tunable diode-laser (TDL) sensor for non-intrusive measurements of the gas temperature and CO_2 concentration behind reflected shock waves.

A. Farooq (✉) · J.B. Jeffries · R.K. Hanson
High Temperature Gasdynamics Laboratory, Department of Mechanical Engineering, Stanford University, Stanford, CA 94305, USA
e-mail: aamir@stanford.edu
Fax: +1-650-7231748

Over the past 25 years, TDL absorption sensors have been used successfully to provide in-situ, time-resolved, line-of-sight measurements of temperature, gas concentration, velocity, density, mass flux, and pressure in a variety of combustion environments [3–7]. Most of these TDL sensors are based on direct absorption techniques due to the relatively simple interpretation of measurement results [3–5, 7, 8]. The tuning rates of many TDLs limit much of the reported scanned-wavelength direct absorption sensor bandwidths to several kHz. Fixed-wavelength direct absorption sensors are limited only by the detector bandwidth but this strategy can be prone to errors for low-absorption applications because of various noise sources such as beam steering, window fouling, and radiative emission. Wavelength modulation spectroscopy with second-harmonic detection (WMS-2f) is a well-known technique for improving the signal-to-noise ratio (SNR) for small amounts of absorption [10–19]. Second-harmonic line shapes reduce the sensitivity to baseline-fitting errors encountered in direct absorption, since they are sensitive to line shape curvature, making them advantageous in dealing with noisy signals and weak absorption levels. Thus, for combustion environments with uniform properties along the measurement line-of-sight like shock-tubes, WMS-2f can be an effective method of yielding temperature measurements with higher accuracy and bandwidth than direct absorption measurements [15]. Fortuitously, for injection-current-tuned TDLs the wavelength modulation is accompanied with simultaneous intensity modulation. This intensity modulation can be exploited to normalize the 2f signal by the 1f signal to account for laser transmission variations due to beam steering, emission, window fouling, and scattering. Such normalization was first introduced in 1982 [9], and its utility has recently been demonstrated in various combustion applications [18–23].

Most previous TDL sensors used robust telecommunications diode lasers and optical fiber technology in the near-infrared (NIR) 1.3–1.6 μm wavelength region. Recent developments in semiconductor diode-laser technology have extended the range of cw room-temperature single-mode diode lasers to 2.9 μm [24], allowing for access to stronger vibrational bands of H_2O, CO_2, NO and other species. Initial development of sensors at these longer wavelengths has been reported [25–27], demonstrating more sensitive measurements of species concentration and temperature. Compared to an early temperature sensor using NIR H_2O transitions in shock-tubes [23], the advantages of working at longer wavelengths (near 2.7 μm) and using CO_2 for measuring the temperature were recently reported in the context of a direct absorption sensor [25]. Here, that work has been extended by incorporating a 1f-normalized WMS-2f strategy and improved hardware to achieve a higher SNR and accuracy of temperature measurements behind reflected shock waves. These experiments also report the first application of the WMS-2f strategy using a new class of diode lasers near 2.7 μm.

In previous work [25], the absorption spectrum of CO_2 near 2.7 μm was systematically analyzed to select an optimal line pair for temperature measurements and the pertinent spectroscopic parameters (line strength, line broadening) for these transitions were measured and validated. Here, the laser modulation depth for each CO_2 transition is optimized to maximize the WMS-2f signal for the targeted shock-tube test conditions. The lasers are then characterized to determine the relevant real-diode-laser parameters for the specific modulation depth and modulation frequency. The sensor is designed to achieve high temperature sensitivity and low sensitivity to cold boundary layer and changes in gas pressure and composition. The fixed-wavelength WMS-2f sensor is then validated under known conditions in a heated static cell and behind reflected shock waves in known CO_2–Ar mixtures. Finally, measurements of CO_2 and temperature are carried out behind reflected shock waves in ignition experiments of heptane–O_2 system to demonstrate the sensor's utility for chemistry measurements. Pre-ignition temperature histories are also measured by seeding a small quantity of relatively inert CO_2 in the initial fuel-oxidizer mixture.

2 Absorption spectroscopy

Direct absorption spectroscopy is chosen for many optical sensors due to its simplicity and ease of data interpretation. Sensor design based on direct absorption spectroscopy has been discussed in detail previously [28, 29], and the notation and units used in this work follow [25].

Wavelength modulation spectroscopy with second-harmonic detection (WMS-2f) is an extension of absorption spectroscopy that has long been used for sensitive species detection and thermometry [10–19]. In this technique, the TDL injection current is rapidly modulated to produce a simultaneous modulation of the laser intensity and wavelength. The second harmonic of the transmitted intensity is a function of the gas conditions and spectroscopic parameters and therefore can be used to make measurements of unknown gas properties. This technique is sensitive to line shape curvature rather than absorption magnitude [30], which is helpful for measurements with low-absorption levels. The TDL injection current is sinusoidally modulated with angular frequency $\omega = 2\pi f$, and the instantaneous laser output frequency $\nu(t)$ can be expressed by

$$\nu(t) = \bar{\nu} + a\cos(\omega t) \tag{1}$$

where $\bar{\nu}$ [cm^{-1}] is the center laser frequency and a [cm^{-1}] is the modulation depth. The diode-laser intensity is simul-

taneously modulated, and the instantaneous laser intensity $I_0(t)$ is given by

$$I_0(t) = \bar{I}_0\left[1 + i_0\cos(\omega t + \psi_1) + i_2\cos(2\omega t + \psi_2)\right] \quad (2)$$

Here $\bar{I}_0$ is the average laser intensity at $\bar{\nu}$, i_0 is the linear intensity modulation (IM) amplitude with phase shift ψ_1, and i_2 is the nonlinear IM amplitude with phase shift ψ_2 [16, 17].

For WMS-2f detection, a lock-in is used to measure the second-harmonic (2f) signal by multiplying the detector signal by a sinusoidal reference signal at frequency 2ω. In WMS measurements, the background 2f signal needs to be measured in the absence of absorption and vector-subtracted from the 2f signal. This background 2f signal comes from the nonlinear laser IM and is often referred to as the residual amplitude modulation (RAM). The magnitude of the absorption-based WMS-2f signal is then given by

$$\begin{aligned} S_{2f}(\bar{\nu}) = \frac{G\bar{I}_0}{2}\Bigg\{\Bigg[H_2 + \frac{i_0}{2}(H_1 + H_3)\cos\psi_1 \\ + i_2\left(H_0 - 1 + \frac{H_4}{2}\right)\cos\psi_2\Bigg]^2 \\ + \Bigg[\frac{i_0}{2}(H_1 - H_3)\sin\psi_1 \\ + i_2\left(H_0 - 1 - \frac{H_4}{2}\right)\sin\psi_2\Bigg]^2\Bigg\}^{1/2} \end{aligned} \quad (3)$$

where G accounts for the optical-electrical gain of the detection system and the later transmission losses due to scattering, beam steering, and window fouling. H_0, H_1, H_2, H_3, and H_4 are components of Fourier series expansion of the transmission coefficient [19]. Similarly, the magnitude of the first-harmonic (1f) signal can be obtained as

$$\begin{aligned} S_{1f}(\bar{\nu}) = \frac{G\bar{I}_0}{2}\Bigg\{\Bigg[H_1 + i_0\left(H_0 + \frac{H_2}{2}\right)\cos\psi_1 \\ + \frac{i_2}{2}(H_1 + H_3)\cos\psi_2\Bigg]^2 \\ + \Bigg[i_0\left(H_0 - \frac{H_2}{2}\right)\sin\psi_1 \\ + \frac{i_2}{2}(H_1 - H_3)\sin\psi_2\Bigg]^2\Bigg\}^{1/2} \end{aligned} \quad (4)$$

The hardware-related parameters and transmission losses can be accounted for by normalizing the absorption-based WMS-2f signal with the WMS-1f signal $C = \frac{S_{2f}}{S_{1f}}$. By this normalization, common terms such as the average laser intensity, detector sensitivity, signal amplification, lock-in gain, and laser transmission variations are eliminated. The 1f-normalized WMS-2f signal is a function of known laser parameters ($i_0, i_2, a, \psi_1, \psi_2$) and gas parameters ($P$, T, and χ_i) only. The laser parameters can be determined before the measurements, and no calibration is needed to scale the simulations to the measurements [16]. In addition to the absorption parameters, the WMS-2f signal also depends on the modulation depth a. The WMS-2f signal can be maximized by choosing the optimum modulation index m, which is defined as

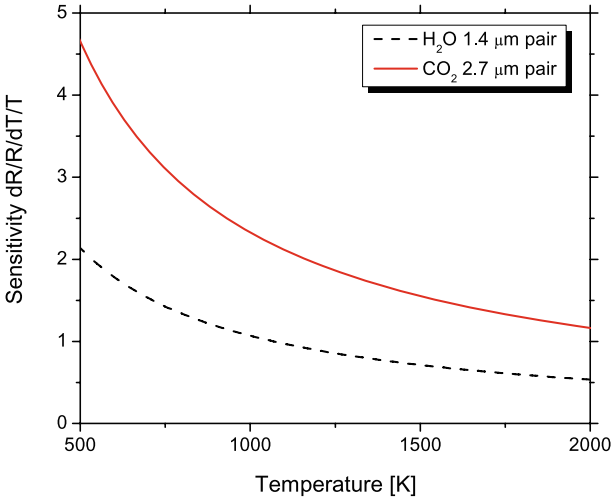

Fig. 1 Comparison of the temperature sensitivity of the current CO_2 line pair near 2.7 μm with the H_2O line pair near 1.4 μm used previously [23]

$$m = \frac{a}{\Delta\nu/2} \quad (5)$$

where $\Delta\nu$ [cm^{-1}] is the full width at half maximum (FWHM) of the absorption line shape.

The gas temperature can be obtained from the ratio of the 1f-normalized WMS-2f signals near the line center of two transitions

$$R = \frac{C_2}{C_1} = \frac{(S_{2f}/S_{1f})_{\bar{\nu}_2}}{(S_{2f}/S_{1f})_{\bar{\nu}_1}} \quad (6)$$

which is closely related to the ratio of absorption line strengths. If the total gas pressure is measured by a pressure transducer, the gas temperature can be inferred from the measured ratio R, using simulations of the ratio as a function of temperature at the measured pressure. The simulated values include the effects of differences in line shape function between the two lines owing to different values of laser modulation parameters and broadening coefficients. After the temperature has become known, the species concentration can be determined from either of the 1f-normalized WMS-2f signals.

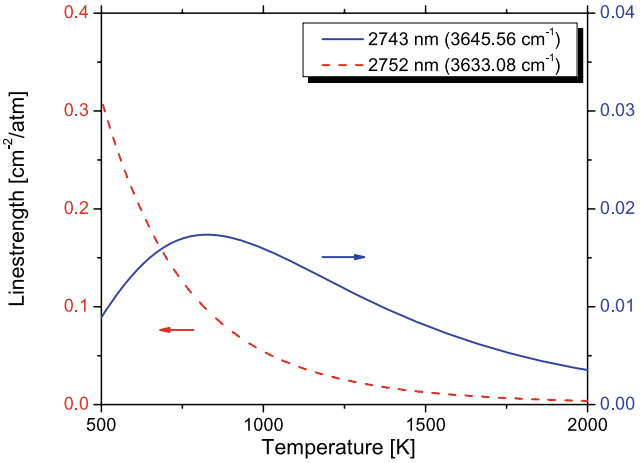

Fig. 2 Measured line strength as a function of temperature for the CO_2 transitions near 2752 and 2743 nm (data taken from [25])

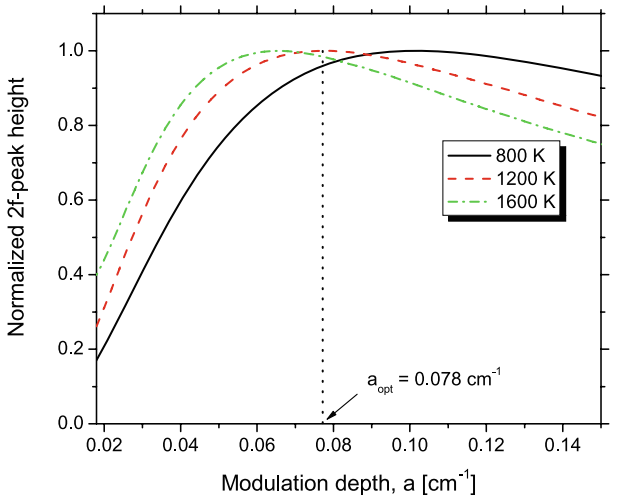

Fig. 3 Simulated normalized WMS-2f peak height for the CO_2 transition near 3633.08 cm^{-1} (2752.48 nm) versus modulation depth a; $P = 1.0$ atm, 1% CO_2 in Ar, $L = 14.13$ cm

3 Sensor design

3.1 Selection of spectral lines

Selection of optimum absorption transitions is the first step in the design of a TDL sensor. A systematic design-rule-based line selection procedure is used to identify optimal transitions for temperature measurement in shock-tubes [25]. The selected transitions belong to the $\nu_1 + \nu_3$ vibrational band of CO_2 and have line centers near 2752.48 and 2743.06 nm, respectively, or equivalently 3633.08 and 3645.56 cm^{-1}. The well-separated lower-state energies (E'') of 316.77 and 1936.09 cm^{-1} enable sensitive temperature measurement over a wide range of temperatures (500–2000 K). The sensitivity, defined here as the unit change in the normalized line strength ratio, $\Delta R/R$, for a unit change in the normalized temperature, $\Delta T/T$, for this line pair is plotted in Fig. 1 along with the sensitivity of the H_2O line pair near 1.4 μm used previously for temperature measurement in shock-tubes [23]. The CO_2 line pair used in this work offers improved temperature sensitivity over the entire temperature range of interest. While the selected transitions work very well for the targeted experimental conditions, it should be emphasized that care must be undertaken while using these transitions for other applications. For example, in cases where cold boundary-layer thicknesses are significant the transition with low E'' should be replaced with a transition that is less sensitive to gas at low temperatures. Similarly for temperature measurements above 2000 K, a line pair with larger $\Delta E''$ should be used to achieve higher sensitivity.

Critical spectroscopic parameters (line strength and collisional broadening coefficient) for the two selected CO_2 transitions have previously been measured [25] and are summarized in Table 1. The measured line strengths agree quite well with the HITRAN database [31, 32] and are plotted in Fig. 2. The Ar-broadening parameters needed for the shock-tube work were not previously listed in any spectroscopic database.

3.2 Optimization of modulation depth

The temperature measurement using WMS-2f is complicated by the dependence of the WMS-2f peak height on the line shape function and the variation of the modulation index, m, with temperature dependence of $\Delta\nu$. This variation can be minimized by tuning the modulation amplitude such that m is near a value of 2.2. The simulated normalized WMS-2f peak height is plotted in Fig. 3 for the CO_2 transition near 3633.08 cm^{-1} versus modulation depth at three temperatures ($T = 800$, 1200, 1600 K), $P = 1.5$ atm, 1% CO_2 in Ar, and path length (L) of 14.13 cm. The simulation is based on a Voigt line shape with the spectroscopic parameters listed in Table 1. At each temperature, the maximum value of the WMS-2f peak signal occurs near $m = 2.2$, as expected [11, 13]. The optimal modulation depth, $a_{opt} = 0.078$ cm^{-1}, is chosen such that the second-harmonic component (H_2) remains relatively constant for the target temperature range of 800–1600 K. Similarly, the optimum modulation depth for the other CO_2 transition near 3645.56 cm^{-1} is determined to be 0.063 cm^{-1} for the range of expected conditions in the shock-tube. By selecting optimum modulation depths, the ratio of two WMS-2f peak heights is dominated by the temperature dependence of the well-known line strengths of the selected absorption features. These modulation depths are selected for temperature measurements in the temperature range of 800–1600 K and pressure range of 1–2 atm. For different temperatures and pressures, the modulation depth can be optimized using the same procedure.

Table 1 Line strengths and line broadening parameters for the two selected CO_2 transitions (from [25]). Measured values are compared with HITRAN 2004 values wherever available. Uncertainties are given in the parentheses

Species	v_0 [cm^{-1}]	E'' [cm^{-1}]	S (296 K) [cm^{-2}/atm]		$2\gamma_{self}$ (296 K) [cm^{-1}/atm]		n	$2\gamma_{CO_2-Ar}$ (296 K) [cm^{-1}/atm]	m
			Measured	HITRAN04	Measured	HITRAN04	Measured	Measured	Measured
CO_2	3633.08	316.77	6.13E–01	5.98E–01	0.171	0.177	0.654	0.112	0.658
			(2%)	(2–5%)	(2.5%)	(2–5%)	(2.2%)	(2.7%)	(2.6%)
CO_2	3645.56	1936.09	7.04E–04	7.12E–04	0.130	0.124	0.695	0.091	0.694
			(2%)	(2–5%)	(2.5%)	(2–5%)	(3.3%)	(2.9%)	(2.9%)

3.3 Characterization of diode lasers

Before making temperature measurements using WMS-2f, a diode laser must be characterized to determine the laser parameters in (2) (i_0, i_2, ψ_1, and ψ_2) for a specific modulation frequency and modulation depth. Two distributed-feedback (DFB) diode lasers (NanoPlus GmbH [24]) operating near 2752 and 2743 nm are modulated by a sinusoidal injection current at 100 kHz with a modulation depth of 0.078 and 0.063 cm^{-1}, respectively. The laser modulation depths are inferred by sinusoidally fitting the fringe centers in the interference pattern produced by a solid Germanium etalon with a free spectral range of 0.016 cm^{-1}. The modulation frequency of 100 kHz gives a maximum sensor bandwidth of 50 kHz set by the low-pass filter of the lock-in amplifier. We find that the laser frequency is well described by a sinusoidal modulation when the diode laser is driven with a pure sine-wave injection current.

The amplitude of laser IM (i_0) is determined by fitting the laser intensity signal without absorption to a sinusoidal function. The FM/IM phase shift (ψ_1) is extracted from the measured modulation of intensity and frequency. When the laser injection current is sinusoidally modulated, the light intensity is nearly simultaneously modulated, with a phase delay in the frequency modulation. Previously it was assumed that this FM/IM phase shift is exactly π [10, 13]; but recent researchers [19, 22] have shown that this phase shift may differ from this value, especially at larger modulation depths. For the lasers and modulation amplitude used in this work, the FM/IM phase shift is measured to be 1.27π for the 2752 nm laser and 1.43π for the 2743 nm laser. These values are somewhat larger than those measured for previous fiber-coupled NIR lasers ($\sim 1.2\pi$) [19]. Clearly, the value of the FM/IM phase shift varies with the specific laser.

The nonlinear intensity modulation term (i_2) is determined from the residual of the 1f fit of the intensity modulation. The residual is nearly sinusoidal at twice the modulation frequency. The nonlinear IM is the source of the background 2f signal, known as residual amplitude modulation (RAM). Although the amplitude of the nonlinear IM is usually small ($\sim 1\%$) compared with that of the linear IM, the induced RAM can be of the same order as the absorption-based 2f signal. There are various methods to mitigate the effect of this background signal. In this work, the RAM signal is measured and vector-subtracted from the 2f signal [23].

Knowing the FM/IM phase shift ψ_1, the phase shift of the nonlinear IM term ψ_2 can also be determined from fitting the laser intensity. When the nonlinear IM term (i_2) is relatively small, the magnitude of the nonlinear phase shift ψ_2 does not play an important role in the overall IM. We find that the measured diode laser IM is well characterized by the combination of 1f and 2f terms, and higher-order terms are not needed.

The normalized laser intensity for the two lasers used in this work is given below for $f = 100$ kHz and $a = 0.078$ cm^{-1}, 0.063 cm^{-1} for the 2752 and 2743 nm lasers, respectively:

$$I_0(t)/\bar{I}_0 = 1 + 0.486\cos(2\pi f t + 1.27\pi) + 0.0053\cos(4\pi f t + 1.35\pi) \quad (7)$$

$$I_0(t)/\bar{I}_0 = 1 + 0.571\cos(2\pi f t + 1.43\pi) + 0.0068\cos(4\pi f t + 1.37\pi) \quad (8)$$

3.4 Pressure sensitivity

For the fixed-wavelength WMS-2f/1f temperature sensor, the laser wavelengths are chosen at the line-center of the two CO_2 transitions, and gas temperature is determined by comparison of the measured WMS-2f/1f signal ratio with simulations at the measured pressure. Although the WMS-2f peak height for an individual transition varies with pressure and temperature as shown in Fig. 4 for the 2752 nm laser, it is desirable that the ratio of WMS-2f peak heights be mainly a function of temperature. Fig. 5 illustrates the WMS-2f signal ratio for the 2752 nm/2743 nm line pair as a function of temperature for various pressures with optimum modulation depths for the two CO_2 transitions (1% CO_2 in Ar). The normalized 2f signal ratio is almost identical for the three pressures over the temperature range of interest. The WMS-2f signal ratio is closely related to the ratio of absorption line

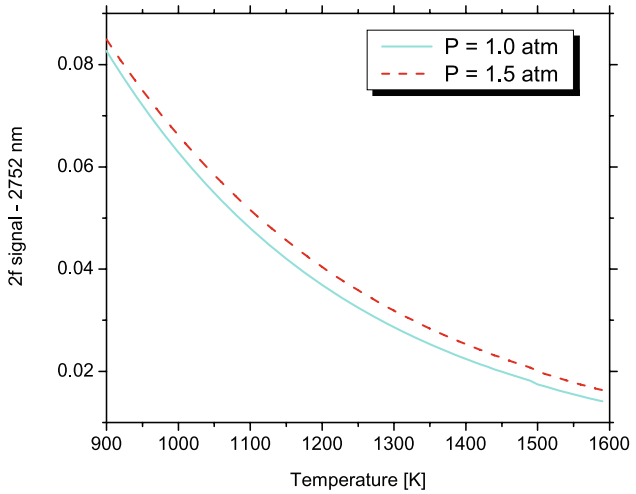

Fig. 4 Simulated WMS-2f peak height for the CO_2 transition near 3633.08 cm^{-1} (2752.48 nm) versus temperature; $a = 0.078$ cm^{-1}, 1% CO_2 in Ar, $L = 14.13$ cm

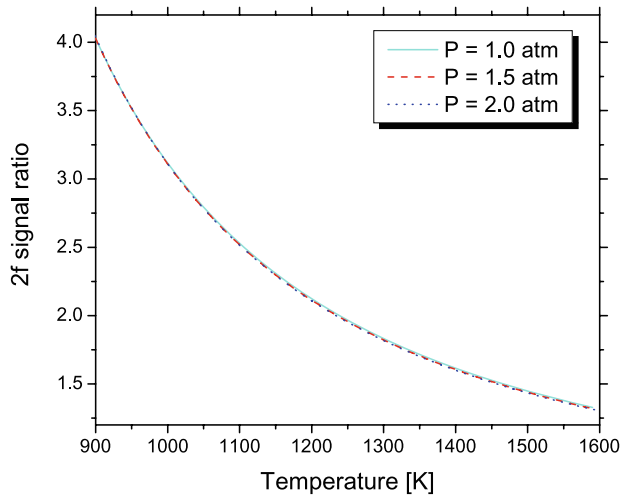

Fig. 5 Simulated WMS-2f signal ratio for the 2752/2743 nm line pair as a function of temperature for various pressures at optimum modulation depths; 1% CO_2 in Ar, $L = 14.13$ cm

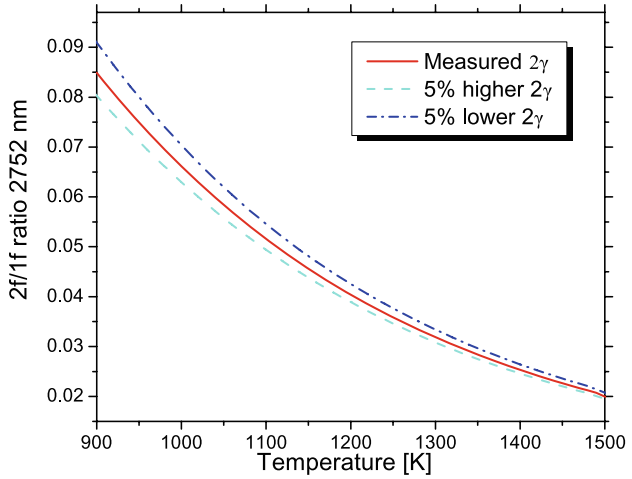

Fig. 6 Simulated WMS-2f/1f ratio for the 2752 nm transition as a function of temperature for three different values of collisional broadening coefficient $2\gamma_{CO_2\text{–}Ar}$

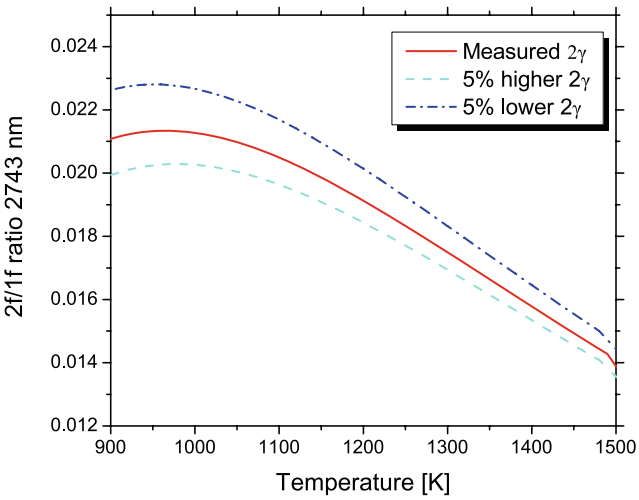

Fig. 7 Simulated WMS-2f/1f ratio for the 2743 nm transition as a function of temperature for three different values of collisional broadening coefficient $2\gamma_{CO_2\text{–}Ar}$

strengths, and is only a weak function of pressure. Thus, the changes in the measured WMS-2f ratio primarily reflect the changes of gas temperature and these measurements are only weakly dependent on the measured pressure.

3.5 Sensitivity to spectroscopic parameters

Since the gas temperature is determined by comparison of the measured WMS-2f signal ratio with simulations based on spectroscopic parameters, the inferred gas temperature depends on these spectroscopic parameters (line strength, line shape). The measured line strength values for the two transitions are well known and agree quite well with the HITRAN database. The line shape data is comprised mainly of Doppler and collisional line widths. The collisional broadening coefficient of CO_2 in Ar ($2\gamma_{CO_2\text{–}Ar}$) is not available in the literature for CO_2 transitions. By fixing the Doppler line width at a specific temperature, $2\gamma_{CO_2\text{–}Ar}$ is measured in well-controlled heated static cell experiments. Uncertainty in the broadening coefficient can either come from its measurement or because of changes in the gas composition, i.e. by having different collision partners. If we consider $2\gamma_{CO_2\text{–}Ar}$ to be the main source of uncertainty in the simulated WMS-2f ratios, the uncertainty in the temperature measurement can be estimated.

Figures 6 and 7 plot the simulated WMS-2f peak heights for the CO_2 transitions near 2752 and 2743 nm respectively using the measured $2\gamma_{CO_2\text{–}Ar}$ (taken from Table 1)

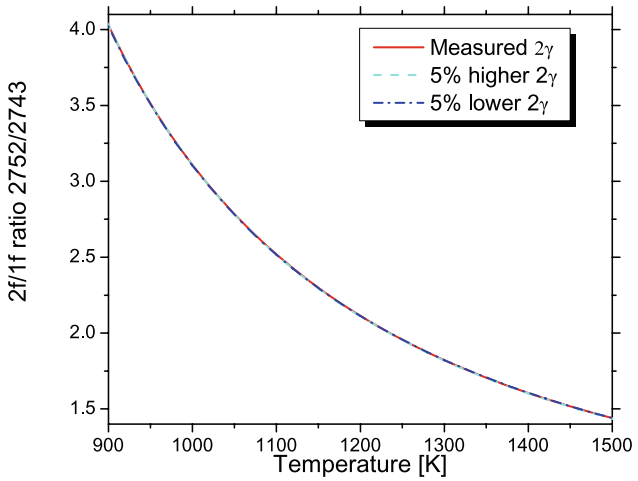

Fig. 8 Simulated WMS-2f/1f ratio for the 2752/2743 nm line pair as a function of temperature for three different values of collisional broadening coefficient $2\gamma_{CO_2\text{–}Ar}$

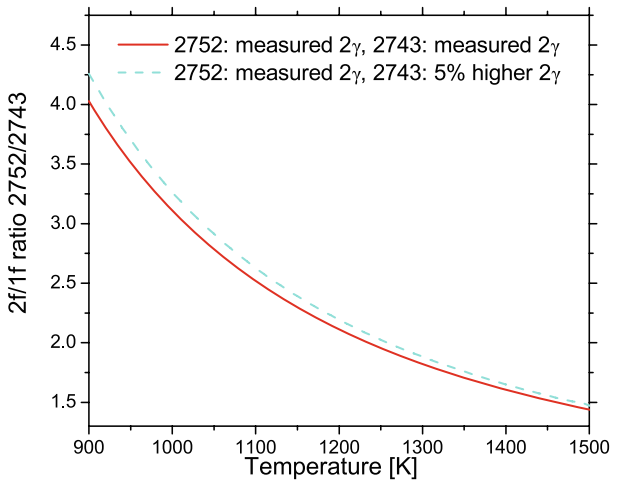

Fig. 9 Simulated WMS-2f/1f ratio for the 2752/2743 nm line pair as a function of temperature for two different cases

as well as using values 5% higher or lower than the measured $2\gamma_{CO_2\text{–}Ar}$. If the $2\gamma_{CO_2\text{–}Ar}$ is increased or decreased by the same percentage for the two transitions, the simulated WMS-2f ratio is not affected (see Fig. 8). However, if we use the measured $2\gamma_{CO_2\text{-}Ar}$ for one transition and higher or lower $2\gamma_{CO_2\text{–}Ar}$ for the other transition the simulated 2f ratio is different than using measured values for both transitions. For the specific case shown in Fig. 9, this discrepancy translates into a measured temperature uncertainty of 25 K at 1200 K. Since the estimated uncertainty in the measured $2\gamma_{CO_2\text{–}Ar}$ and its temperature coefficient is less than 3% [25], the maximum uncertainty caused by line shape parameters in the measured WMS-2f temperature is predicted to be less than 2%.

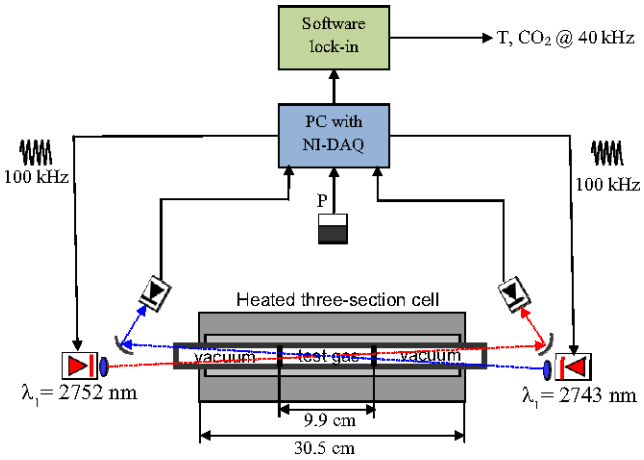

Fig. 10 Schematic diagram of the experimental setup used for WMS-2f sensor validation in a heated static cell

4 Sensor validation in heated static cell

The fixed-wavelength WMS-2f temperature sensor is first tested in the well-controlled environment of a heated static cell; the arrangement of the experiment is shown in Fig. 10. The laser beams are transmitted through a three-section optical cell by collimating parabolic mirrors and the signals are collected on liquid-nitrogen-cooled InSb detectors (IR Associates IS-2.0, 1 MHz). The cell is mounted with CaF_2 windows wedged at 3° angle to avoid unwanted interference fringes. The cell is placed inside a heated furnace, and the 9.9 cm center section of the cell is filled with test gas and located in the uniform-temperature region of the furnace, while the two outer sections are evacuated to avoid any interference by ambient CO_2 and avoid any temperature gradients near the ends of the tube furnace. Three type-K thermocouples (Omega) are equally spaced along the center section of the heated cell to determine the temperature of gas samples, the maximum temperature difference observed between the thermocouples is <1%. Cell pressure is measured by a 100 Torr/10000 Torr capacitance manometer (MKS 620A/627B) with an accuracy of ±0.12% of reading.

The two DFB lasers are mounted in commercial laser mounts and their wavelength is varied by a combination of temperature and injection current using commercial controllers (ILX Lightwave LDT-5910B and LDX-3620). The lasers are tuned to the line center wavelengths 2752.48 nm (3633.08 cm^{-1}) and 2743.06 nm (3645.56 cm^{-1}) of the two probed CO_2 transitions R(28) and P(70) respectively, using a free-space mid-IR wavelength meter (Bristol 621). The two diode lasers are sinusoidally modulated by 100 kHz digital waveforms generated by a PC running a 10 MHz National Instruments data acquisition (NI-DAQ) system. The modulation depths are adjusted near the optimum values, as discussed in Sect. 3.2. The detector signals are recorded at 10 MHz using the same computer. The detector signal is demodulated by a digital lock-in program on LabView with a

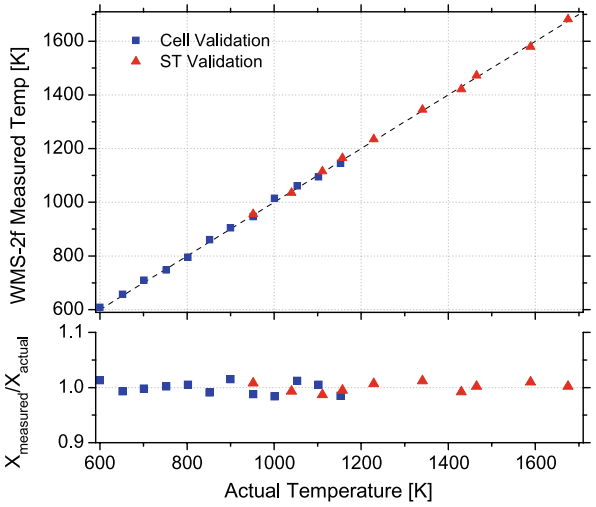

Fig. 11 Validation measurements of the fixed-wavelength WMS-2f sensor. The *square points* represent the validation experiments carried out in the heated static cell ($P \sim 1$ atm, 2% CO_2 in Ar, $L = 9.9$ cm). The *triangular points* represent the validation experiments carried out in the shock-tube ($P_5 \sim 1$–2 atm, 2% CO_2 in Ar, $L = 14.13$ cm)

low-pass filter bandwidth of 40 kHz to extract the 1f and 2f signals. Our previous shock-tube temperature sensor [23] utilized an infinite impulse response (IIR) digital filter (e.g. 8th order Butterworth filter), whereas this work uses an improved finite impulse response (FIR) digital filter. The impulse response of an FIR filter is 'finite' because it settles to zero in a finite number of sample intervals. This is in contrast to the IIR filters, which have internal feedback and may continue to respond indefinitely.

The heated static cell is evacuated before each experiment and the background 1f signals and 2f signals (X- and Y-components for vector subtraction) are recorded for each laser. The cell is then filled with a 2% CO_2–Ar mixture to $P \sim 1$ atm, and the 1f and 2f (X- and Y-components) signals with absorption are recorded for each laser. The background-subtracted 1f-normalized WMS-2f signals are calculated using

$$\left(\frac{2f}{1f}\right)_{meas} = \sqrt{\left(\frac{2f_x}{1f} - \frac{2f_{xbg}}{1f_{bg}}\right)^2 + \left(\frac{2f_y}{1f} - \frac{2f_{ybg}}{1f_{bg}}\right)^2} \quad (9)$$

These measured values are compared with simulated 2f/1f values to infer the gas temperature and the CO_2 mole fraction. The top panel of Fig. 11 (square points for static cell) compares the thermocouple measurements with the temperatures from the fixed-wavelength WMS-2f temperature sensor; the bottom panel shows the ratio of the CO_2 mole fraction measured by the TDL sensor and the known mixture mole fraction. All the values plotted in Fig. 11 are averaged over 1 ms. The temperatures determined from the TDL WMS-2f sensor are in excellent agreement with the thermocouple readings over the entire temperature range (600–1200 K) with a standard deviation of 9 K. The TDL measured CO_2 mole fractions are also in good agreement with known mixture values with a standard deviation of 1.2%. The improved sensitivity and accuracy achieved with this sensor points to the advantages of working at longer wavelengths and utilizing the WMS-2f absorption strategy.

5 Sensor validation in non-reactive shock-tube experiments

The shock-tube provides a well-controlled transient environment to test the sensor performance. The WMS-2f CO_2 sensor is tested in non-reactive CO_2–Ar mixtures behind reflected shock waves. Experiments are performed in the reflected-shock region of a high-purity, stainless-steel shock-tube regularly used in our laboratory for kinetics studies [33, 34]. The shock-tube inner diameter is 14.13 cm, and the driven section is 8.54 m in length, separated from the driver section by a polycarbonate diaphragm. Under normal shock-tube conditions, the driver section is 3.35 m long and helium is used for the driver gas. This geometric configuration provides 2–3 ms of high-quality test time of uniform temperature and pressure. This test time is limited by either the arrival of rarefaction waves from the driver section, or reflected shock-contact surface interactions near the test section. Recently, the test time of the shock-tube has been extended to ~20 ms for measurements at lower temperatures by making two modifications: (1) the driver section is lengthened to a total of 6.4 m to allow more time before the arrival of the rarefaction fan in the test section, and (2) tailored driver gas mixtures of 30 to 40% N_2 in He are used to minimize shock wave-contact surface interactions. In some experiments, we have also utilized a new strategy of modifying the shock-tube by inserting a properly designed cone-shaped obstacle into the driver section of the shock-tube, as a means of generating more constant reflected-shock conditions [35, 36]. The temperature and pressure behind the reflected shock waves are calculated using standard normal-shock relations and the measured incident shock speed [37]. The incident shock speeds are determined from time-interval measurements from a series of five pressure transducers spread over the final 1 m of the shock-tube and linearly extrapolated to the shock-tube end wall.

TDL measurements are made at a location 2 cm from the end wall, and the experimental setup is illustrated in Fig. 12 to show the cross section of the shock-tube and optical/electronics arrangement. The light from each laser is collimated and transmitted through optical windows on the shock-tube side wall. The optical arrangement is based on the assumption that the gas properties across the shock-tube are uniform as expected for heating by a planar shock. As in cell experiments, the two diode lasers are modulated

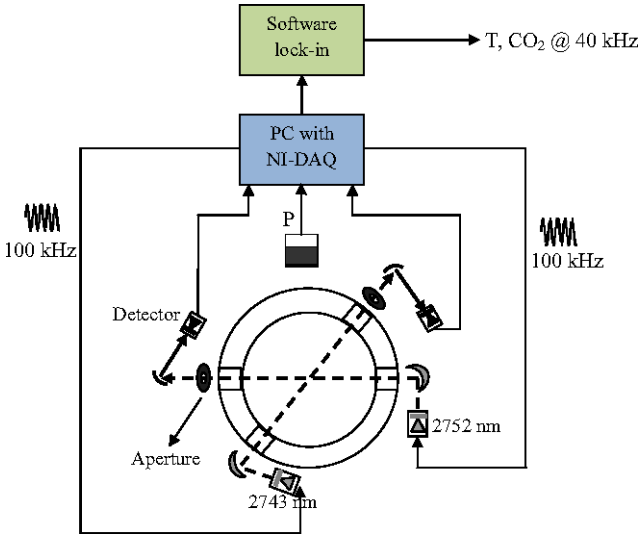

Fig. 12 Schematic diagram of the experimental setup used for WMS-2f sensor measurements in the shock-tube

by 100 kHz digital waveforms and the modulation depths are adjusted close to the optimum values. The test procedure is similar to the one described for static cell validations. Prior to each experiment, the shock-tube is evacuated by a turbomolecular pump to an ultimate pressure of $\sim 3 \times 10^{-6}$ Torr to record the background 1f and 2f (X- & Y-components) signals for both lasers. The shock-tube is then filled with CO_2–Ar mixture to $P_1 = 20$–70 Torr. The data acquisition system is triggered by the pressure transducer to record the pressure and transmitted 1f and 2f signals for both CO_2 lasers during the shock-heating process. The time histories of gas temperature and CO_2 concentration are then inferred by comparing the background-subtracted 1f-normalized WMS-2f signals with simulated values. Top panel in Fig. 13 plots the WMS-2f/1f signals for the two lasers behind a shock with 2% CO_2 in Ar at reflected-shock conditions of $T_5 = 952$ K and $P_5 = 1.197$ atm using a tailored driver gas of 40% N_2 in He. These two 2f/1f signals are used to compute the temperature time history plotted in the bottom panel of Fig. 13 along with the measured pressure. The average measured temperature over the time interval 0–8 ms is 955.2 K which is in excellent agreement with the value calculated from the ideal shock equations, $T_5 = 952$ K. The relatively large CO_2 absorption strength near 2.7 μm and the use of the WMS-2f/1f strategy provides higher accuracy, better sensitivity and excellent SNR (than achieved previously [23]) as demonstrated in the difference plot (Fig. 14) of measured T and calculated T_5. The standard deviation of ~3 K at the measured temperature of 952 K translates to an uncertainty of only 0.32%. CO_2 mole fraction can be computed using the measured pressure, temperature and transmission signal of either laser. The measured mole fraction is plotted in Fig. 15 for the same shock and is in excellent agreement with the known mixture value of 2%.

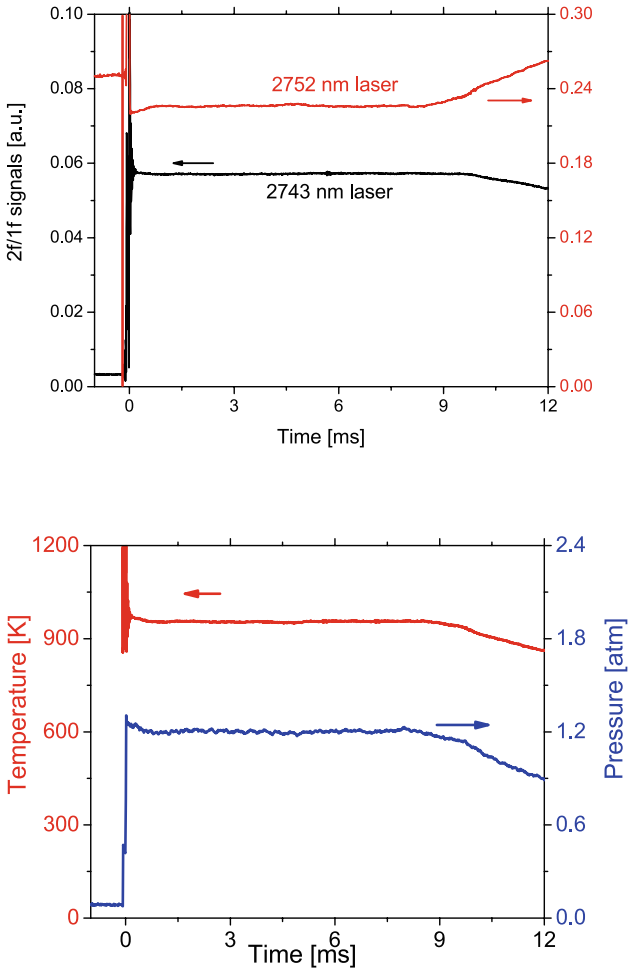

Fig. 13 *Top panel*: measured WMS-2f/1f signals for the two lasers behind a reflected shock wave arriving at $t = 0$. Reflected shock conditions 952 K, 1.20 atm, 2% CO_2 in Ar, tailored driver 40% N_2 in He with driver insert. *Bottom panel*: measured temperature and pressure

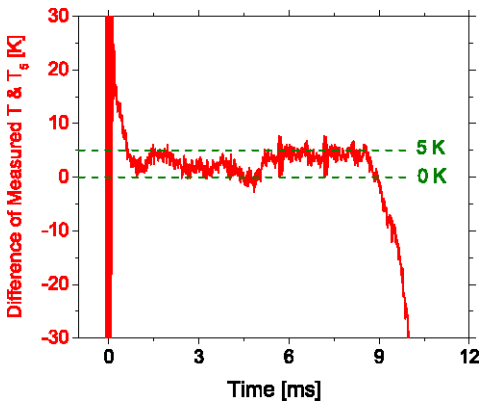

Fig. 14 Difference in measured T and calculated T_5 (reflected shock temperature) for the same shock as in Fig. 13

Similar tests are performed at different temperatures by varying the initial fill pressure (P_1). The results are plotted in Fig. 11 (triangular points for shock-tube) where the

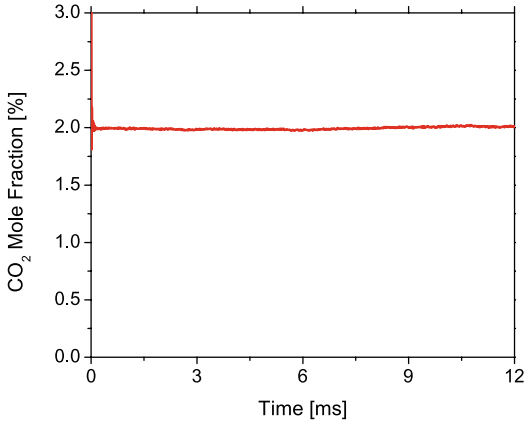

Fig. 15 CO_2 mole fraction measured by the WMS-2f sensor during the same shock as Fig. 13

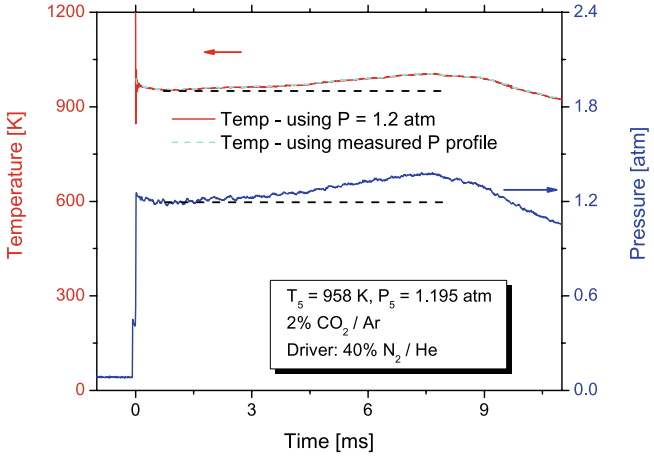

Fig. 16 Measured temperature and pressure behind reflected shock wave arriving at $t = 0$. Reflected shock conditions 958 K, 1.20 atm, 2% CO_2 in Ar, tailored driver 40% N_2 in He. (The two plotted temperature profiles are almost identical.)

top panel compares the measured WMS-2f sensor temperature with that calculated from ideal shock relations (T_5), and the bottom panel compares the measured CO_2 mole fraction with known mixture values. The measured and calculated temperatures are in excellent agreement (within <1%) over the tested temperature range, 900–1700 K, and the measured mole fraction agrees with the mixture values within 1.1%. These results validate the sensor accuracy and response for temperature and CO_2 concentration measurements at combustion temperatures and illustrate the potential for applications in combustion studies with varying temperature and mole fractions.

The temperature measurement by the WMS-2f sensor is not sensitive to the noise in the measured pressure (as discussed in Sect. 3.4). Thus, the noise in the temperature measurement comes mostly from the laser/detection system and the measured temperature follows the actual conditions in the shock-tube very closely. The pressure insensitivity of the 2f temperature sensor is demonstrated in Fig. 16 for a shock that shows appreciable dP/dt owing to the removal of driver inserts. From the measured 1f-normalized WMS-2f signal the temperature is calculated in two ways: (a) compare with simulated 2f/1f using a constant pressure of $P = 1.2$ atm, (b) compare with simulated 2f/1f using a measured pressure profile. These two methods result in nearly identical temperature profiles, confirming that the diagnostic is not sensitive to pressure variations.

In shock-tube experiments with very little energy release, it is generally assumed that the post-shock temperature follows the pressure isentropically. This has been verified here by temperature measurements using WMS-2f in CO_2/Ar shocks; a typical case is shown in Fig. 17, where the measured temperature profile is plotted along with temperature calculated using isentropic compression:

$$\left(\frac{T_{\text{calculated}}}{T_5}\right) = \left(\frac{P_{\text{measured}}}{P_5}\right)^{\frac{\gamma-1}{\gamma}}, \quad \gamma_{\text{Ar+CO}_2} = 1.654$$

While analyzing the accuracy of this temperature diagnostic, the existence of boundary layers in shock-tubes should also be considered. Boundary-layer growth in shock-tubes has been extensively studied and several numerical models have been developed to quantify this growth [38–40]. Since TDL sensing is a line-of-sight measurement and provides a path-averaged temperature measurement, the cold boundary layer in the laser path can cause some uncertainty in the measured temperature of the core flow, particularly when either of the transitions being used has low E''. For the shock-tube used in this work with diameter of 14.13 cm, numerical simulations [40] indicate that the maximum possible thickness of boundary layer is 1 mm at the typical pressure and temperature range of this work and for the test times of interest. Since the laser measurements are carried out through the shock-tube side-wall, the laser passes through the boundary layer twice and thus travels a total distance of 2 mm through the cold boundary layer. The objective is to estimate the uncertainty in temperature measurement that could be produced by the boundary layer for the particular case of the post-shock data shown in Fig. 13, where the temperature calculation assumed that the entire 14.13 cm path-length is at a uniform temperature. Now if we redo the calculation by making a simplifying assumption that 2 mm of that path-length is at room temperature (297 K) for both lasers, we get a new 2f/1f simulated ratio that is 0.9% different. This translates into a temperature uncertainty of 3.5 K or 0.36% for the reflected-shock temperature of 952 K. This demonstrates that the cold boundary layer has negligible impact on the temperature measurements using WMS-2f sensor and the measured temperature accurately describes the core flow temperature.

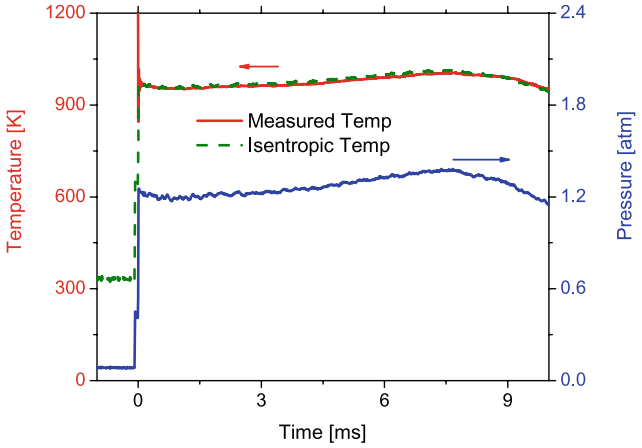

Fig. 17 Comparison of the measured temperature with isentropic temperature. Reflected shock conditions are same as in Fig. 16

6 Sensor application in reactive shock-tube experiments

The development of detailed reaction mechanisms to describe high-temperature combustion chemistry relies on an array of experimental tests or kinetic targets for validation and refinement. Shock-tubes provide nearly ideal test beds for computational validation of these mechanisms. While ignition delay times provide an overall measure of the performance of kinetic mechanisms, refinement and validation of the detailed chemistry of the system requires understanding of the time-dependent temperature and species concentrations, including reactants, intermediates, and products. Non-intrusive optical diagnostic techniques such as laser absorption and infrared emission are ideal for such measurements.

Here, we use the WMS-2f CO_2 sensor to measure temperature and CO_2 time histories in the combustion of a heptane-O_2 mixture. Commercially available heptane (>99% pure) from Sigma–Aldrich and research grade O_2/Ar/He/N_2 supplied by Praxair Inc. are used in the experiments. Mixtures are prepared by partial pressures in a stainless-steel mixing chamber equipped with a magnetic stirrer assembly and allowed to mix overnight. The mixing assembly and shock-tube driven section are maintained at room temperature. The optical setup is similar to that shown in Fig. 12. The measured temperature and CO_2 mole fraction are plotted in Fig. 18 for a shock with 0.25% heptane and 2.75% O_2 in Ar (equivalence ratio $\phi = 1$) as the initial mixture and reflected-shock conditions of $P_5 = 1.8$ atm and $T_5 = 1361$ K. The measured temperature profile is obtained after CO_2 starts forming at the ignition event (~0.7 ms). The measurement results are compared with simulations performed using the JetSurf kinetic mechanism [41] in conjunction with a simple reactive gas dynamics model (CHEMSHOCK) [42]. Reliable measurements under combustion conditions further establish confidence in this new sensor strategy and indicate that the diagnostic is not affected by interference from hydrocarbon species and other products of combustion.

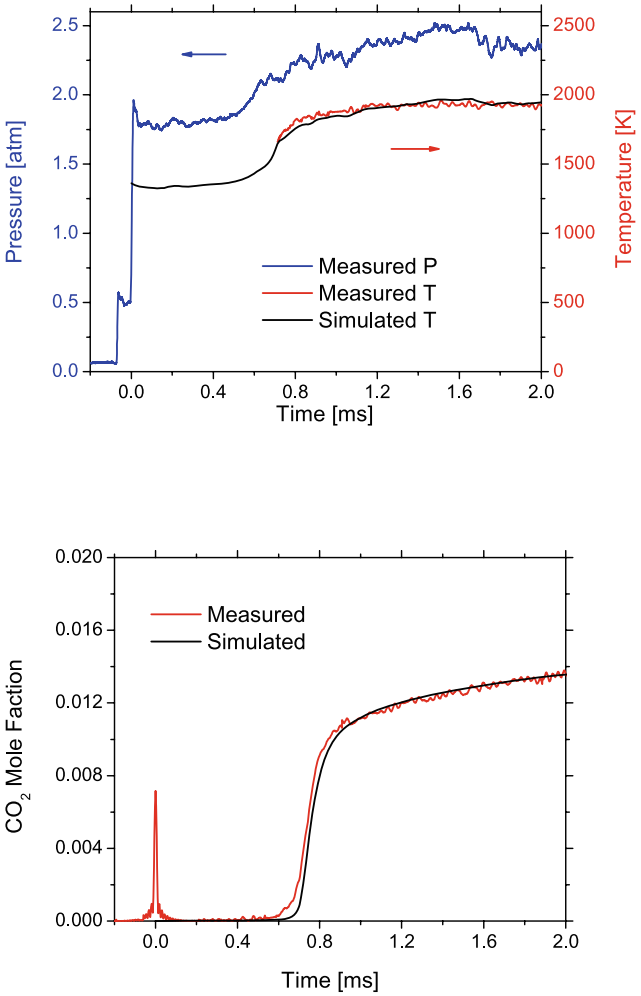

Fig. 18 *Top panel*: measured temperature and pressure behind reflected shock wave. Mixture: 0.25% heptane, 2.75% O_2, balance Ar. Reflected shock conditions: $T_5 = 1361$ K, $P_5 = 1.8$ atm. *Bottom panel*: measured CO_2 mole fraction for the same shock. Simulations are based on the JetSurf kinetic mechanism [41]

For the case shown in Fig. 18, the temperature measurement is made after the ignition takes place, as this is when CO_2 is first formed as a combustion product. In order to obtain the pre-ignition temperature profile, CO_2 can be seeded in the initial mixture, as CO_2 is relatively inert and does not perturb the chemistry. An example is shown in Fig. 19 where 1% CO_2 is seeded in a stoichiometric mixture of 0.25% heptane in O_2/Ar, and temperature is measured for the entire test sequence. This temperature information can be quite helpful in understanding pre-ignition chemistry and gas dynamic effects. Measurements of CO_2 profile and temperature can be made for a variety of fuels and hydrocarbons, and we expect that such data will greatly aid validation of existing kinetic mechanisms and for developing more accurate combustion mechanisms.

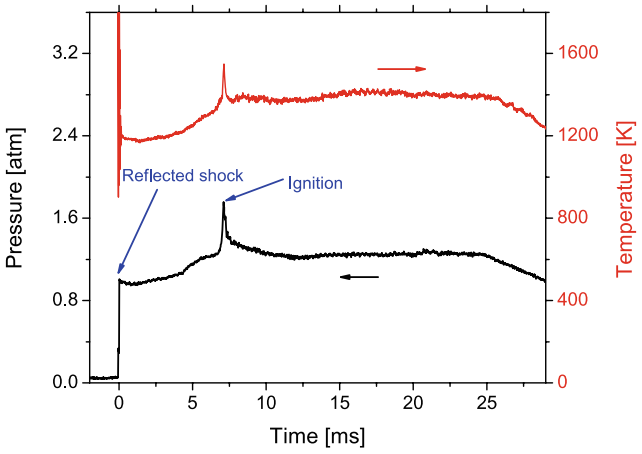

Fig. 19 Measured temperature and pressure behind reflected shock wave. Mixture: 0.25% heptane, 2.75% O_2, 1% CO_2, balance Ar. Reflected shock conditions: 1172 K, 0.98 atm, tailored driver gas with 40% N_2 in He

7 Summary

A new tunable diode-laser sensor for measuring temperature behind reflected-shock waves using wavelength modulation spectroscopy with second-harmonic detection (WMS-2f) is reported. The sensor probes the R(28) and P(70) transitions of the $\nu_1 + \nu_3$ combination vibrational band of CO_2 near 2.7 μm. This band offers absorption strengths that are 1000 and 50 times stronger than the CO_2 bands near 1.5 and 2.0 μm, respectively. The well-separated lower-state energies of the selected transitions enable sensitive temperature measurement over a wide range of temperatures (500–2000 K). Pertinent spectroscopic parameters for these transitions have been previously measured. The two lasers are sinusoidally modulated at 100 kHz and their modulation depths are optimized to maximize the WMS-2f signal for the target conditions in the shock-tube ($P \sim$ 1–2 atm, $T \sim$ 800–1600 K). The lasers are characterized for actual laser performance to determine laser parameters (i_0, i_2, ψ_1, and ψ_2) for the specific modulation frequency and modulation depth. The laser wavelengths are fixed near the line centers to achieve fast time response (∼50 kHz). The WMS-2f signal is normalized by the 1f signal to remove the need for calibration and account for laser transmission variations due to beam steering, emission, window fouling, and scattering. The sensor has negligible sensitivity to pressure variations in the pressure range of interest (1–2 atm). The existence of a cold boundary layer in the shock-tube and changes in gas composition do not induce significant uncertainty to the temperature measurements. The fixed-wavelength WMS-2f sensor is validated in heated static cell experiments and the measured temperatures agree well with thermocouple readings, with a standard deviation of 9 K. Temperatures measured by the TDL sensor agree with calculated reflected shock temperatures within 1% in non-reactive CO_2–Ar shocks. The measured CO_2 mole fractions are also in excellent agreement with known mixture values. Measurements of CO_2 and temperature are subsequently carried out behind reflected shock waves in ignition experiments of heptane–O_2 system. Pre-ignition temperature histories are also measured by seeding a small quantity of relatively inert CO_2 in the initial fuel-oxidizer mixture. The sensor offers improved temperature sensitivity, better accuracy, and excellent SNR owing to the relatively large CO_2 absorption strength near 2.7 μm and the use of 1f-normalized WMS-2f strategy.

Acknowledgements This research is sponsored by the Aerospace, Chemical and Material Sciences Directorate of the Air Force Office of Scientific Research (AFOSR), with Dr. Julian Tishkoff manager of the Combustion and Diagnostics Program as technical monitor.

References

1. I. Glassman, *Combustion* (Academic Press, San Diego, 1996)
2. R.K. Hanson, D.F. Davidson, in *Handbook of Shock Waves*, ed. by G. Ben-Dor, O. Igra, T. Elperin, vol. 1 (Academic Press, San Diego, 2001), Chap. 5.2
3. J.A. Silver, D.J. Kane, P.S. Greenberg, Appl. Opt. **34**, 2787 (1995)
4. H. Teichert, T. Fernholz, V. Ebert, Appl. Opt. **42**, 2043 (2003)
5. M.G. Allen, Meas. Sci. Technol. **9**, 545 (1998)
6. R.K. Hanson, J.B. Jeffries, in *25th AIAA Aerodynamic Measurement Technology and Ground Testing Conference*, Washington, DC (2006), AIAA-2006–3441
7. D. Richter, D.G. Lancaster, F.K. Tittle, Appl. Opt. **39**, 4444 (2000)
8. S.T. Sanders, J.A. Baldwin, T.P. Jenkins, D.S. Baer, R.K. Hanson, Proc. Combust. Inst. **28**, 587 (2000)
9. D.T. Cassidy, J. Reid, Appl. Opt. **21**, 1185 (1982)
10. L.C. Philippe, R.K. Hanson, Appl. Opt. **32**, 6090 (1993)
11. J. Reid, D. Labrie, Appl. Phys. B **26**, 203 (1981)
12. J. Wang, M. Maiorov, D.S. Baer, D.Z. Garbuzov, J.C. Connolly, R.K. Hanson, Appl. Opt. **39**, 5579 (2000)
13. J.T.C. Liu, J.B. Jeffries, R.K. Hanson, Appl. Phys. B **78**, 503 (2004)
14. P. Kluczynski, O. Axner, Appl. Opt. **38**, 5803 (1999)
15. J.A. Silver, D.J. Kane, Meas. Sci. Technol. **10**, 845 (1999)
16. J.A. Silver, Appl. Opt. **31**, 707 (1992)
17. T. Aizawa, Appl. Opt. **40**, 4894 (2001)
18. T. Fernholz, H. Teichert, V. Ebert, Appl. Phys. B **75**, 229 (2002)
19. H. Li, G.B. Rieker, X. Liu, J.B. Jeffries, R.K. Hanson, Appl. Opt. **45**, 1052 (2006)
20. T. Iseki, H. Tai, K. Kimura, Meas. Sci. Technol. **11**, 594 (2000)
21. R.T. Wainner, B.D. Green, M.G. Allen, M.A. White, J. Stafford-Evans, R. Naper, Appl. Phys. B **75**, 249 (2002)
22. G.B. Rieker, H. Li, X. Liu, J.T.C. Liu, J.B. Jeffries, R.K. Hanson, M.G. Allen, S.D. Wehe, P.A. Mulhall, H.S. Kindle, A. Kakuho, K.R. Sholes, T. Matsuura, S. Takatani, Proc. Combust. Inst. **31**, 3041 (2007)
23. H. Li, A. Farooq, J.B. Jeffries, R.K. Hanson, Appl. Phys. B **89**, 407 (2007)
24. Nanosystem and Technologies GmbH, http://www.nanoplus.com
25. A. Farooq, J.B. Jeffries, R.K. Hanson, Appl. Phys. B **90**, 619 (2008)
26. A. Farooq, J.B. Jeffries, R.K. Hanson, Meas. Sci. Technol. **19** (2008)

27. K. Wunderle, S. Wagner, V. Ebert, in *Laser Applications to Chemical, Security and Environmental Analysis*, St. Petersburg, FL (2008), LACSEA-LMB1
28. D.S. Baer, V. Nagali, E.R. Furlong, R.K. Hanson, M.E. Newfield, AIAA J. **34**, 489 (1996)
29. V. Nagali, S.I. Chou, D.S. Baer, R.K. Hanson, Appl. Opt. **35**, 4026 (1996)
30. J.T.C. Liu, J.B. Jeffries, R.K. Hanson, Appl. Opt. **43**, 6500 (2004)
31. L.S. Rothman, D. Jacquemart, The 2004 edition of the HITRAN compilation, in *8th HIITRAN Database Conf.*, Boston: Harvard-Smithsonian Center for Astrophysics, 2004
32. HITRAN website, http://cfa-www.harvard.edu/HITRAN/
33. J.T. Herbon, R.K. Hanson, D.M. Golden, C.T. Bowman, Proc. Combust. Inst. **29**, 1201 (2002)
34. M.A. Oehlschlaeger, D.F. Davidson, R.K. Hanson, J. Phys. Chem. A **108**, 4247 (2004)
35. Z. Hong, G.A. Pang, S.S. Vasu, D.F. Davidson, R.K. Hanson, The use of driver inserts to eliminate facility effects behind reflected shock waves. In preparation
36. Z. Hong, G.A. Pang, S.S. Vasu, D.F. Davidson, R.K. Hanson, Analysis of contact surface tailoring conditions in shock-tubes. In preparation
37. G. Emanuel, in *Handbook of Shock Waves*, vol. 1, ed. by G. Ben-Dor, O. Igra, T. Elperin (Academic Press, San Diego, 2001), Chap. 3.1
38. H. Mirels, in *Shock-Tube Research, Proceedings of the Eighth International Shock-Tube Symposium*, ed. by J.L. Stollery, A.G. Gaydon, P.R. Owen (Chapman & Hall, London, 1972), pp. 6/2–30
39. K.J. Badcock, Int. J. Numer. Methods Fluids **14**, 1151 (1992)
40. E.L. Petersen, R.K. Hanson, AIAA J. **41**, 1314 (2003)
41. B. Sirjean et al., A high-temperature chemical kinetic model of n-alkane oxidation, JetSurf version 0.2 (http://melchior.usc.edu/JetSurF/Version0_2/Index.html) (2008)
42. H. Li, Z.C. Owens, D.F. Davidson, R.K. Hanson, Int. J. Chem. Kinet. **40**, 189 (2008)